Journal of Structural Geology, Vol. 8, No. 5, pp. 527 to 542, 1986
Printed in Great Britain

0191-8141/86 $03.00 + 0.00
Pergamon Journals Ltd.

Grain boundary migration and fabric development in experimentally deformed octachloropropane

M. W. JESSELL

Department of Geological Sciences, State University of New York at Albany, 1400 Washington Avenue, Albany, NY 12222, U.S.A.

(*Received* 2 *January* 1985; *accepted in revised form* 22 *July* 1985)

Abstract—In this study in-situ observations of a deforming aggregate of the hexagonal material octachloropropane have been analysed. Calculations of micro-strains and measurement of *c*-axis orientations have enabled the processes influencing fabric development to be distinguished, and the importance of dynamic recrystallization to be assessed. It was found that, in this material, inter-grain strain contrasts could be large, and the effect of grain boundary migration was to modify the fabric in a measurable way. A simple model for the driving force for grain boundary migration based on dislocation density contrasts, as controlled by intra-grain strains and grain orientations, is proposed and tested, with an 80% success rate for the mobile grain boundaries studied.

INTRODUCTION

THE INTERPRETATION of crystal fabrics in rocks, although debated from the time of Sander on, has not reached a stage at which a given fabric can be demonstrated to have been generated by a single deformation, or even by a range of deformational histories. Current models are based on the rotations associated with crystal plastic glide (Etchecopar 1977, Lister *et al.* 1978); however these have not proved useful in regions of more than the simplest deformation history. The importance of dynamic recrystallization to fabric development has been discussed (Lister & Price 1978, Friedman & Higgs 1981, Urai *et al.* in press); to date, however, the only available evidence has come from naturally deformed samples and rock deformation experiments, which both suffer from the drawback that they do not provide direct evidence of the deformation processes which modify fabrics.

The in-situ observation of deformation processes in polycrystalline aggregates was pioneered in the early 1960s (Wakahama 1964), and has recently been independently expanded by several workers (Tungatt & Humphreys 1981, Means 1983, Urai 1983, Wilson 1984). These authors focused on the identification and study of deformation processes, and made limited calculations of the local strains found within the materials studied. The present work extends the scope of studies relating to dynamic recrystallization by carrying out detailed analyses of inter-grain and intra-grain strains, grain boundary migrations and the progressive reorientations of crystal lattices. The material used in this study was octachloropropane (C_3Cl_8), hereafter called OCP. It is hexagonal, and thus these experiments provide useful information relating to the deformation of materials of low crystallographic symmetry.

EXPERIMENTAL TECHNIQUE

The basic technique is a minor modification of that described in Means (1983). A few mg of laboratory grade OCP are placed in a crucible and mixed with approximately 0.05 weight per cent of silicon carbide grit with an average particle size of 1 μm. The grit is used to mark material positions in the OCP. This mixture is heated to 165°C, just above its melting temperature, vigorously blended, and then allowed to cool. To further distribute the grit through the OCP, the mixture is then chopped finely using a razor blade.

Two glass slides with subparallel frosted grips ground into them are coated with a very thin film of silicone oil, one of the grips having been ground with a slight obliquity so that a small normal stress is applied across the specimen in the plane of the glass glides. This was found to inhibit cracking along grain boundaries. A small quantity of the chopped OCP mix is placed between the slides and the assembly is put in a press at room temperature until the desired sample thickness is achieved. While still in the press the assembly is heated to 80°C until a large enough grain size develops, typically one to two hours for a grain size of 0.17 mm. The end product of sample preparation is a pancake of polycrystalline OCP, approximately 60 μm thick, with a radius of about 1 cm. The region of 'active' specimen between the grips is approximately 1.4 mm wide.

The experiments described in this paper were all carried out at room temperature using the Hajeck press (Means & Xia 1981), which supplies a length-parallel translation to the top slide, which, by means of the frosted grips, imparts a grip-parallel simple shear to the specimen, Fig. 1. The conditions of deformation for the experiments described in this paper are presented in Table 1. Photomicrographs in plain and cross-polarized light were taken at regular intervals, so that the strain

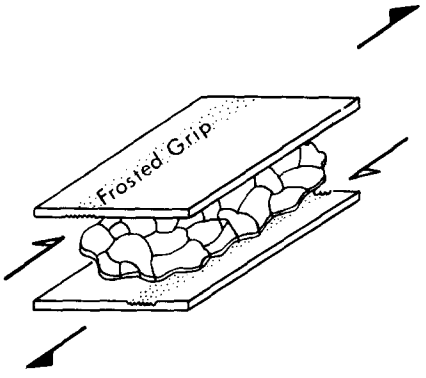

Fig. 1. Geometry of the deformation apparatus. Filled arrows show the relative translation of the glass slides, open arrows show the sense of shear induced in the specimen.

Table 1. Conditions of deformation for experiments described in this paper

	TO-63	TO-64	TO-65
Temperature	Room	Room	Room
Imposed shear strain rate	$4.5\times10^{-5}s^{-1}$	$4.5\times10^{-5}s^{-1}$	$4.5\times10^{-5}s^{-1}$
Duration of experiment	13 hours	2 hours	2 hours
Finite shear strain	1.62	0.64	0.64
Time between photographs	2 hours		1 hour
Time between U-stage measurements	2 hours	2 hours	2 hours

increments between photographs were approximately constant. Crystallographic orientations of the grains were measured on a universal stage by removing the sample from the deformation apparatus for intervals of up to one hour. The experiments described here lasted anywhere from two to thirteen hours, depending on the number of imposed strain increments. At the completion of each experiment the sample was unloaded and left to recover at room temperature.

EXPERIMENTAL OBSERVATIONS

The microstructural response of OCP to the imposed simple shearing was essentially similar from one experiment to another, so it is possible to give a composite description of its behaviour, based on one experiment, TO-63.

At the completion of sample preparation, the grain boundaries were straight or smoothly curved (Fig. 2a), with most grains having no optical subgrain boundaries, and an absence of a grain-shape foliation. However as a result of the hot and cold pressing, a crystallographic preferred orientation had been introduced into the material, which can be characterized by a broad girdle of *c*-axes, the normal to the girdle being parallel to the frosted grips.

Soon after the specimen was loaded, grain boundary migration commenced (Fig. 2b), and characteristically resulted in serrated boundaries, with a wavelength typically on the order of 0.01 mm. Such boundaries remained throughout the period of the experiment.

Experiments that were continued to high strains invariably developed a high strain zone adjacent to one of the frosted grips, and the microstructures that developed in this zone were markedly different from those in the rest of the specimen. The position of this zone is demonstrated in Figs. 2(a)–(e) by the displacement of selected marker particles, marked by stars. Since the imposed bulk strain-rate is constant, the formation of this zone of high strain-rate results in a lowering of the strain-rate in the material elsewhere. The ratio of strain-rates in the two zones was about five to one.

In the zone of lowered strain-rate, grain boundary migration continued and was accompanied by the formation and subsequent migration of subgrain boundaries. A common type of subgrain formation was the development of several subgrain boundaries parallel to the *c*-axis of the host grain; a good example of this can be seen in the grain about 0.1 mm down from the upper-right star in Fig. 2(c). A grain-shape foliation develops; however its maximum lies at about 50° to the shear plane and thus lags nearly 20° behind the orientation of maximum finite elongation.

In contrast the high strain-rate zone is characterized by a rapidly transforming fabric. A grain-shape foliation develops, but is quickly degraded by the actions of grain boundary migration and subgrain formation. A crystallographic preferred orientation develops, marked by a zone of grains with *c*-axes aligned in the plane of the specimen in orientations nearly normal to the shear direction. In Fig. 2(e) this shows up as a band of dark grains adjacent to the upper frosted grip.

In all the experiments there is a gradual widening of the high strain-rate zone. In particular, experiment TO-47 (not otherwise described here but run at the same strain-rate and temperature as those experiments in Table 1), which was allowed to continue to a shear strain of nine, produced a high strain-rate zone that spread laterally across the whole width of the specimen. As a consequence, the strain-rate in the widening zone must have been dropping. As the zone widened the associated zone of near single-crystal preferred orientation widened with it. It is not clear whether the change in strain-rate is stimulating fabric development, or whether the geometrically softened material is causing a local increase in the strain-rate.

After each experiment, complete recovery of grain shapes was achieved, coupled with extensive grain growth, resulting in straight, or smoothly curved grain boundaries forming after six to eight hours (Fig. 2f). Undulatory extinction within grains was also absent after this time. The average grain size was larger than at any stage in the experiment, and the crystallographic fabric was modified, with the zone of near single-crystal fabric sometimes disappearing because grains outside this zone grew preferentially into the material in it. Relatively few optical subgrains remained after one day and after a week continued recovery removed even these.

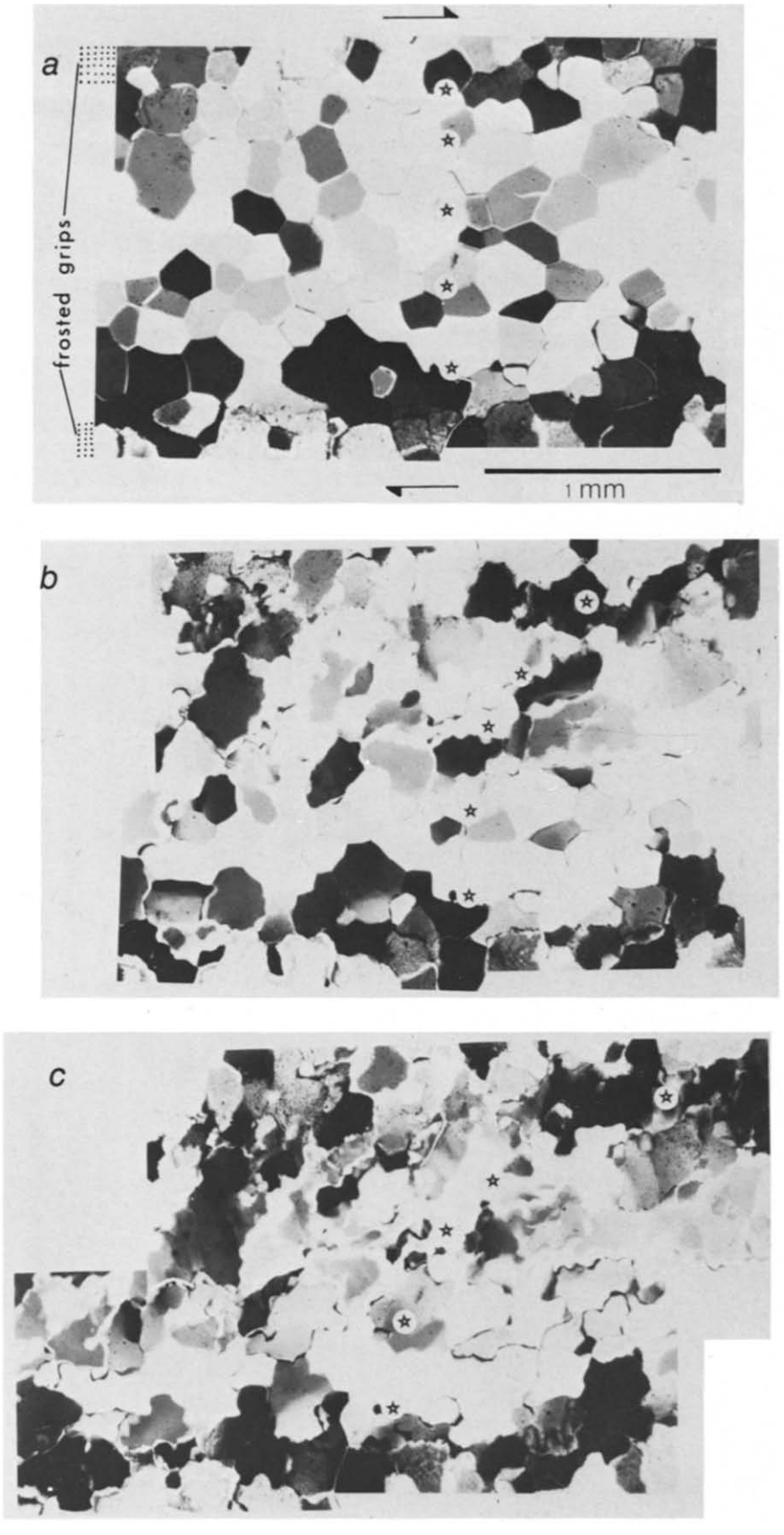

Fig. 2. Photographic record of experiment TO-63, taken at average finite shear strains of (a) 0, (b) 0.25, (c) 0.5.

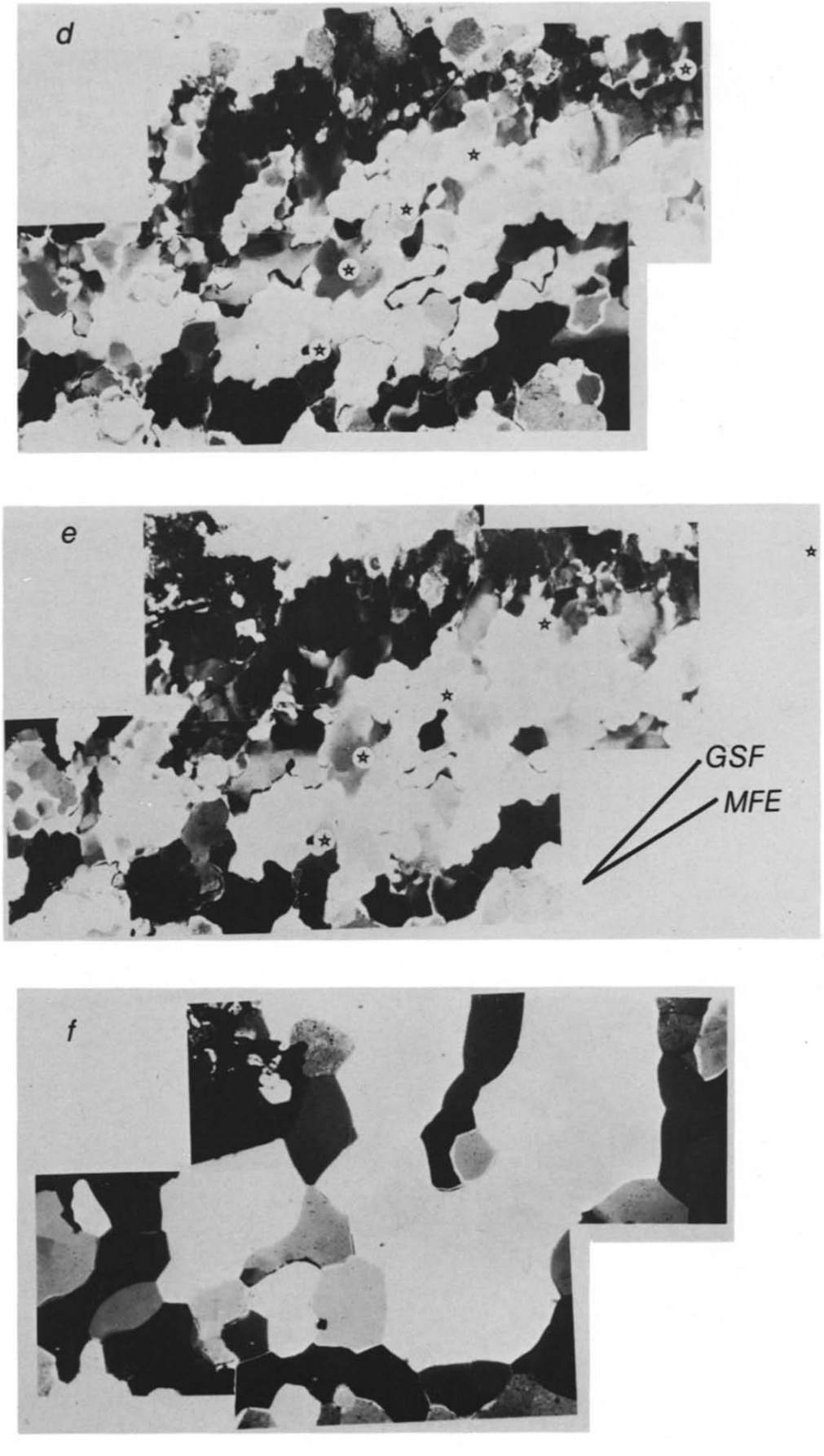

Fig. 2. (*continued*) (d) 0.75, (e) 1.0 and (f) 1.0 (after 10 h of static recovery). Stars show the position of specific marker particles. The obliquity of the grain shape foliation and the orientation of maximum finite elongation are demonstrated in 2(e).

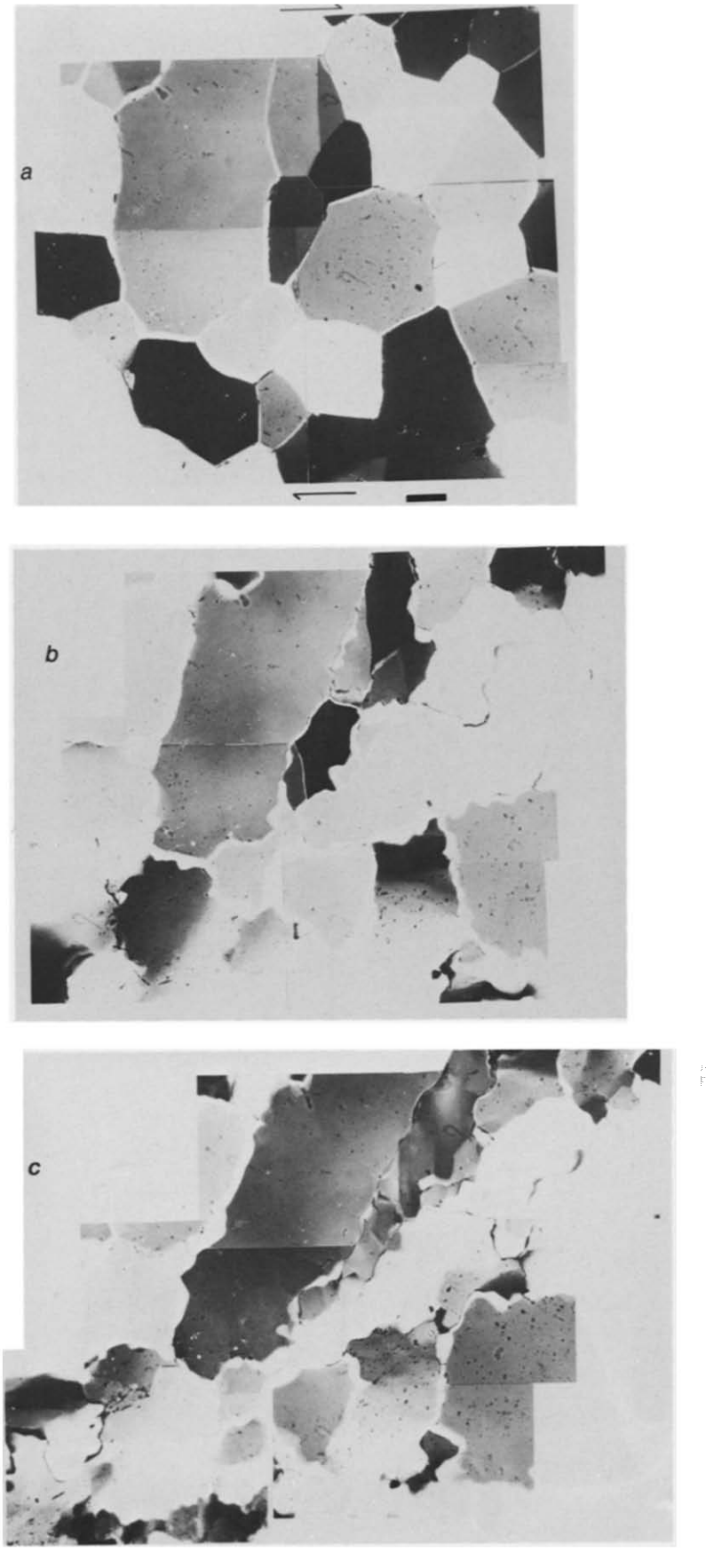

Fig. 8. Photographic record of experiment TO-65, with average finite shear strains of (a) 0, (b) 0.3, (c) 0.6. Scale bar represents 0.1 mm. Marker particles show up clearly as black specks in these photographs.

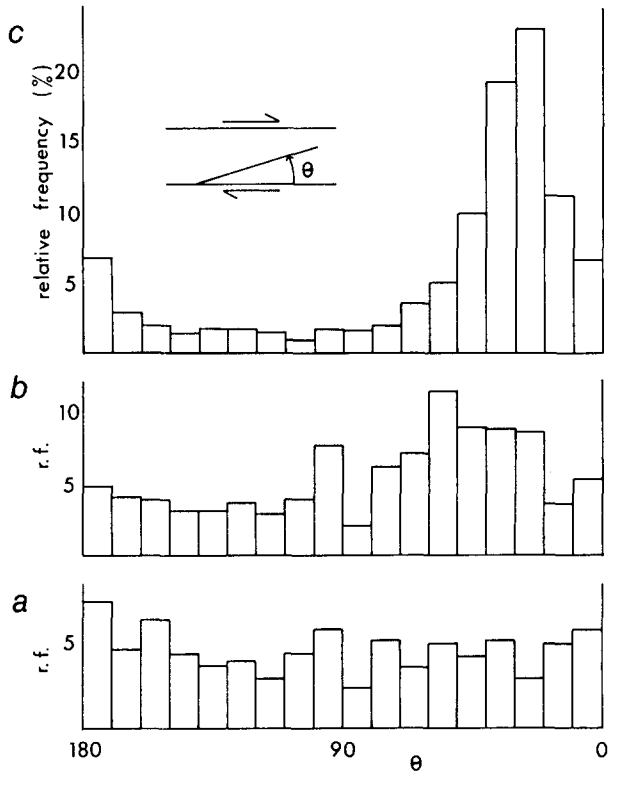

Fig. 3. Histograms of grain boundary segment orientations for experiment TO-63. (a) Frequency distribution of undeformed specimen (416 grain boundary segments). (b) Frequency distribution of same material area in low-strain rate zone after being deformed to a shear strain of one (387 grain boundary segments). (c) Predicted frequency distribution of same material area assuming that the boundaries had acted as passive material lines.

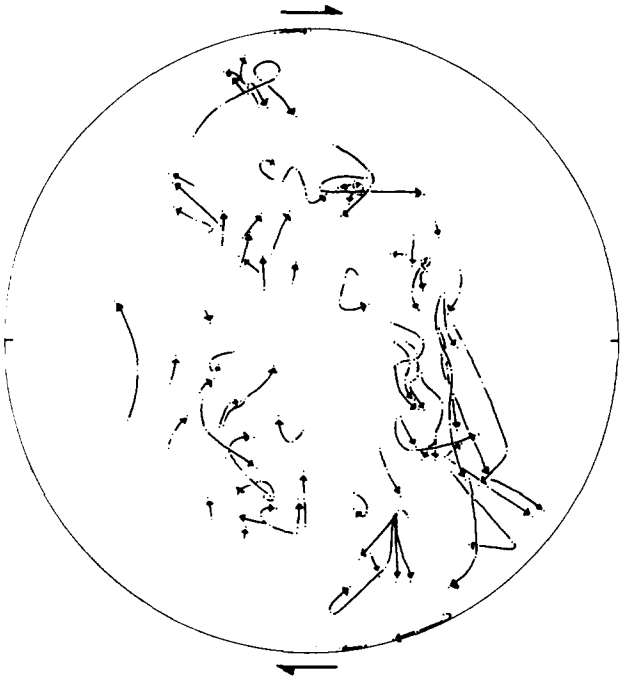

Fig.4. *c*-axis reorientation trajectories for four increments of deformation, plotted on a lower hemisphere equal-area net (experiment TO-63). Each point on a trajectory represents a measured *c*-axis orientation.

ANALYSIS OF EXPERIMENTS

Experiment TO-63

This experiment was undertaken so that an attempt could be made to isolate the effects of grain boundary migration on fabric development. The conditions of deformation are shown in Table 1.

As stated in the previous section, there was a non-parallelism between the orientation of maximum finite elongation and the grain-shape foliation that developed. In order to characterize this obliquity a map of the grain boundaries was traced from the photomicrographs of the low strain-rate parts of the specimen in the undeformed and deformed states, that is at average shear strains of 0 and 1. Individual grain boundaries were then divided into short segments and the orientations of these segments were measured. Figure 3(a) is the relative frequency histogram of these orientations for the undeformed state, and demonstrates that no significant grain shape foliation was present. Figure 3(b) shows that a maximum develops at about 50° from the shear plane after a shear strain of one and Fig. 3(c) shows the grain shape foliation that would have been expected to develop had the grain boundaries acted as passive material lines, for a dextral shear of one. It can be seen that the real foliation has a broader flatter peak that is offset about 20° from the predicted maximum.

In order to analyse the effects of grain boundary migration on lattice orientations the reorientations of individual grains were studied. In total 94 grains were measured, however not all the grains could be followed throughout the experiment, since some were consumed as the experiment progressed, and others were outside the original study area.

When the sequential orientations of each grain are plotted (Fig. 4), a clear pattern of reorientation emerges. In general the *c*-axes of individual grains track a clockwise path around the specimen normal. When optical subgrains develop, this is reflected in the *c*-axis trajectories as an apparently random scattering of 5–10°. However once the subgrains have formed they follow the same clockwise path found for whole grains.

Grain boundary migration produces the terminations of trajectories seen on this plot because of consumption by neighbouring grains. To enable the effects of grain boundary migration to be examined, *c*-axis plots were drawn for each stage of the experiment with the points being replaced by circles proportional to the area of each grain (Figs. 5a–f). In order to estimate the orientations of the six grains that were not measured because they were outside the initial study area, a *c*-axis trajectory diagram, like Fig. 4, compiled from a number of experiments was used, and since the reorientation trends are remarkably consistent for a given orientation, this should not have introduced too large an error.

After the final increment of deformation a pattern of orientations had developed that could be characterized by a double girdle oblique to the shear plane, with a point maximum approximately in the plane of the specimen and normal to the shear direction. This pattern, although weak due to the small final grain population,

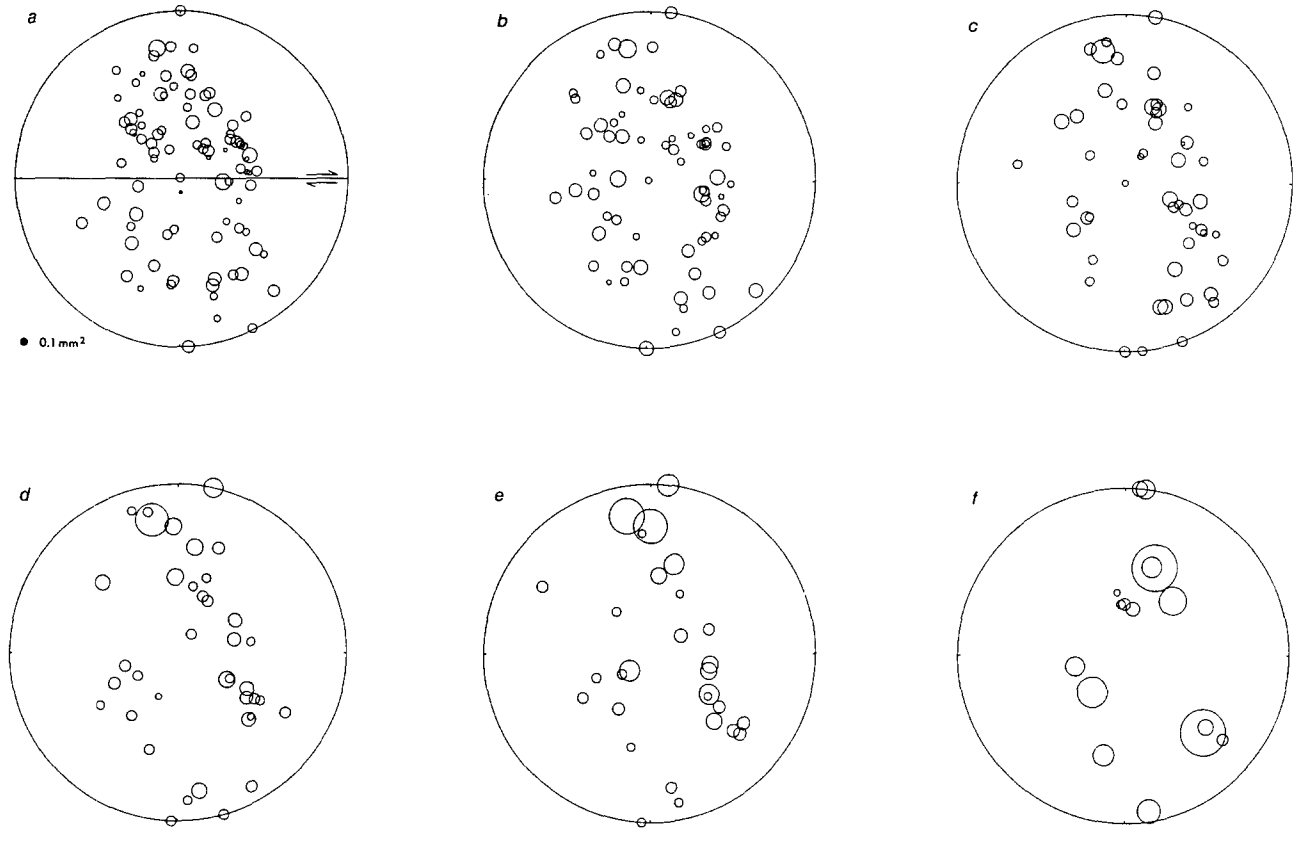

Fig. 5. c-axis fabric diagrams for each stage of the deformation, with circles drawn proportional to grain areas (experiment TO-63). A 0.1 mm^2 scale circle is shown in (a) (solid dot). (a)–(f) represent the same stages of the experiment as shown in Figs. 2(a)–(f).

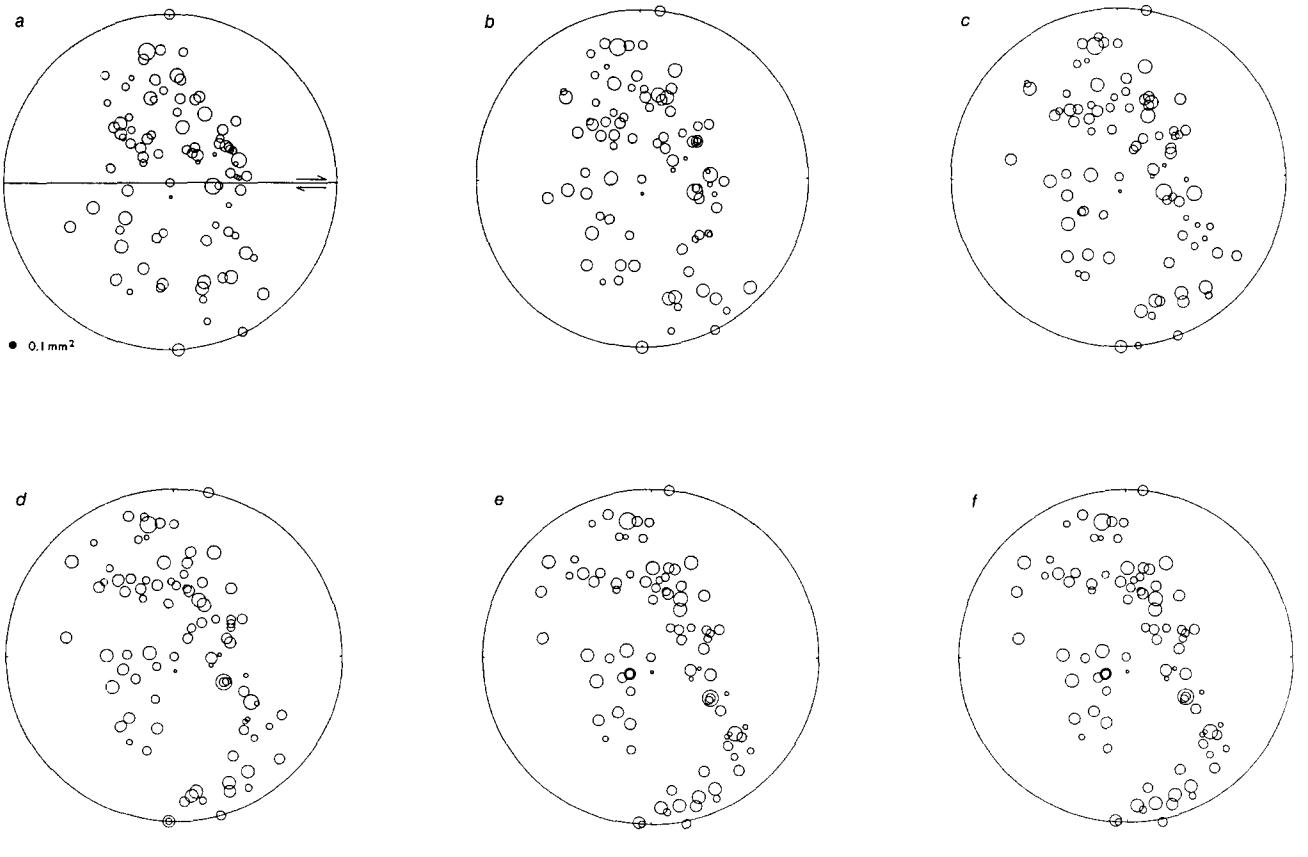

Fig. 6. Theoretical c-axis fabric diagrams calculated by assuming no grain area changes and average c-axis trajectories for experiment TO-63. Compare with Fig. 5.

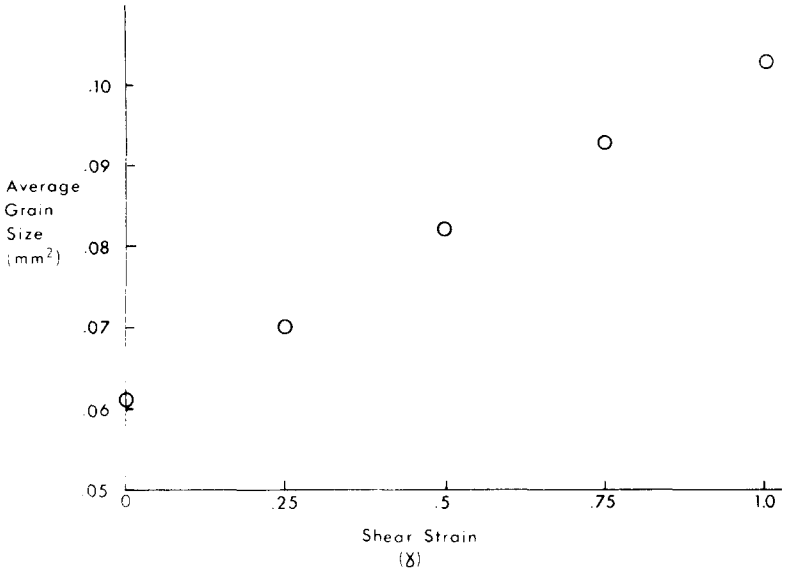

Fig. 7. Graph of average grain size vs shear strain in the low-strain rate zone for experiment TO-63.

has been repeated in another experiment. The point maximum and oblique girdle are similar to examples from naturally deformed quartzites and ice (Hudleston 1980, Jensen 1984, fig. 7c). As the future orientations of grains could be predicted from their present orientations, using a composite reorientation diagram, it was possible to calculate the grain area/orientation diagrams that would have developed had no grain area changes taken place (Figs. 6a–f). Comparing this sequence with the real fabric diagrams (Figs. 5a–f), it can be seen that grain area changes produced the point maximum that developed in this experiment. The processes likely to affect grain areas are grain boundary migration, with or without long-range diffusion, and conversion of subgrains into grains by progressive misorientation. The measured area change within the plane of the specimen was small, and consistent from one grain to the next. Furthermore the transformation of subgrains into grains was rare, so this leaves grain boundary migration as the major cause of grain area changes.

The average grain area in this experiment was found to increase linearly with shear strain in the low strain-rate zone (Fig. 7). Thus the higher the strain the greater the area of material oriented by grain boundary migration. Furthermore, in these experiments, except possibly in the high strain-rate zone, a microstructural steady state had not been reached. The deformation-induced grain growth implies that the steady state grain size for the imposed stress is considerably above the starting grain size, and this is a reversal of the usually observed experimental situation, and also of the case normally assumed for naturally deforming rocks, although Twiss (1977) suggested that the approach to a steady state grain size for quartz in this situation may be very slow. The grain size stress relationship (Mercier *et al.* 1977) implies that in regions where the stress is weakening and a steady-state grain size has been established, grain growth should occur, and thus these experiments may model the late stage of fabric development in orogens, the period that may sometimes be preserved in the fabrics of naturally deformed rocks. The experiment shows the modifying effect of grain boundary migration on fabric development, however it does not provide many clues to grain boundary dynamics.

Experiments TO-64 and TO-65

These experiments were undertaken in order to produce strain maps showing the orientations and magnitudes of the principal strains, together with the new positions of material lines. Data was analysed from both experiments, but examples will be drawn only from TO-65. The photographic record of this experiment is shown in Figs. 8(a)–(c).

Strain analysis

The information provided by the change in shape of a triangle defined by a specific triad of marker particles at two stages of the deformation allows a local deformation matrix to be calculated, if the assumption of homogeneous strain is made (Fig. 9). Defining one of the three particles as the local origin allows two simple sets of equations to be written,

$$\begin{pmatrix} a & b \\ c & d \end{pmatrix}\begin{pmatrix} X_1 \\ Y_1 \end{pmatrix} = (X_1' \;\; Y_1') \text{ and } \begin{pmatrix} a & b \\ c & d \end{pmatrix}\begin{pmatrix} X_2 \\ Y_2 \end{pmatrix} = (X_2' \;\; Y_2'),$$

where (X_1, Y_1) and (X_2, Y_2) are the positions of the particles in the undeformed state, relative to the local origin, (X_1', Y_1') and (X_2', Y_2') are their respective positions in the deformed state and

$$\begin{pmatrix} a & b \\ c & d \end{pmatrix}$$

is the matrix that transforms the initial triangle into the new one.

This set of equations can readily be rearranged as two sets of simultaneous equations,

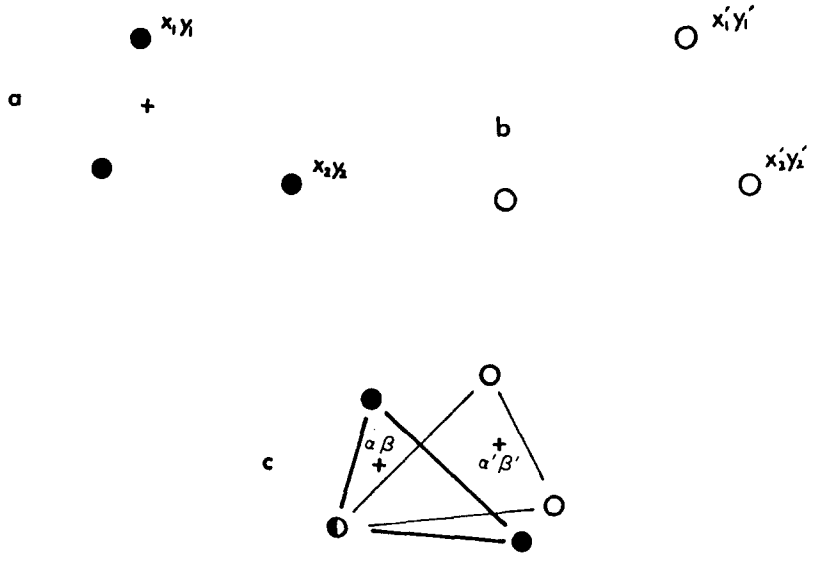

Fig. 9. Information used to calculate local deformation matrices. (a) Marker particles in undeformed state, (b) particles in deformed state and (c) two states superimposed making one of the particles the local origin. The cross represents an arbitrary material point (α, β coordinates) in the undeformed state whose position (α', β') in the deformed state is calculated using the deformation matrix.

$$X_1 \cdot a + Y_1 \cdot c = X_1'$$
$$X_2 \cdot a + Y_2 \cdot c = X_2'$$
and
$$X_1 \cdot b + Y_1 \cdot d = Y_1'$$
$$X_2 \cdot b + Y_2 \cdot d = Y_2'.$$

Once these simultaneous equations have been solved, the assumption of homogeneous strain allows the position of any material point within the initial triangle to be calculated in the deformed state.

By superimposing an imaginary square grid on the undeformed photograph a reference state can be defined by the grid intersections. At each grid point in the undeformed state the three closest marker particles that form a triangle enclosing the grid intersection are chosen, and found again in the deformed state. Effecting the calculations described above gives the strain matrix for the chosen triangle and from this the interpolated position of the grid intersection in the deformed state can be calculated. For each grid intersection the orientation and magnitude of the principal strains can also be calculated from the strain matrix, as described in Ramsay (1967, pp. 60–63).

The first stage of analysis was to record the positions of the grit marker particles using a sonic digitiser coupled to a Univac 1100/83 computer. Figure 10(a) shows the orthogonal grid in the undeformed state, superimposed on a map of the grain boundaries for experiment TO-65, and Fig. 10(b) shows the calculated shape of the grid in the deformed state, together with the new positions of grain boundaries.

Restricting marker triangles to those in which all three particles are within the same grain results in a loss of data at grain boundaries, but ensures that the calculated strains are not affected by any possible grain boundary sliding. Figure 10(c) shows the intra-grain strain maps for experiment TO-65. Each grid square was 0.03 mm on a side in the undeformed state. Small fluctuations in the smoothness in the interpolated positions of material points in the deformed state are of the same order of magnitude as the errors introduced when the data is digitized, and widely displaced grid intersections are nearly always the result of the Fortran program having chosen three virtually co-linear points for the triangle surrounding a grid point in the undeformed state. Strain calculations using such flat triangles proved to be completely unreliable, so average strain calculations that were made ignored these data.

Although intra-grain strains are not perfectly homogeneous, they generally vary smoothly. In contrast it can be seen that inter-grain strain contrasts are of a significantly greater magnitude. No strain contrasts could be reliably associated with subgrain boundaries. Mean stretches in individual grains were calculated by averaging stretches for each grid intersection. The overall average stretch of 1.37 in TO-65 included individual grains having a range of stretches from 1.08 to 1.85. There was an overall area reduction in the plane of the specimen of 5%, which can probably be ascribed to the specimen thickening normal to the plane of the slides as a result of the slight obliquity of one of the frosted grips. Throughout the material there is a general increase in strain from the top of the specimen to the bottom, with the edge of an incipient high strain-rate zone being visible at the very bottom.

Grain boundary kinematics

The review paper by Urai *et al.* (in press) identifies four driving forces for grain boundary migration, namely chemical energy, grain boundary energy, stress induced elastic strain energy and lattice defect energy. Presumably chemical energy can be ruled out in a single phase polycrystal, if any impurities are assumed to be evenly

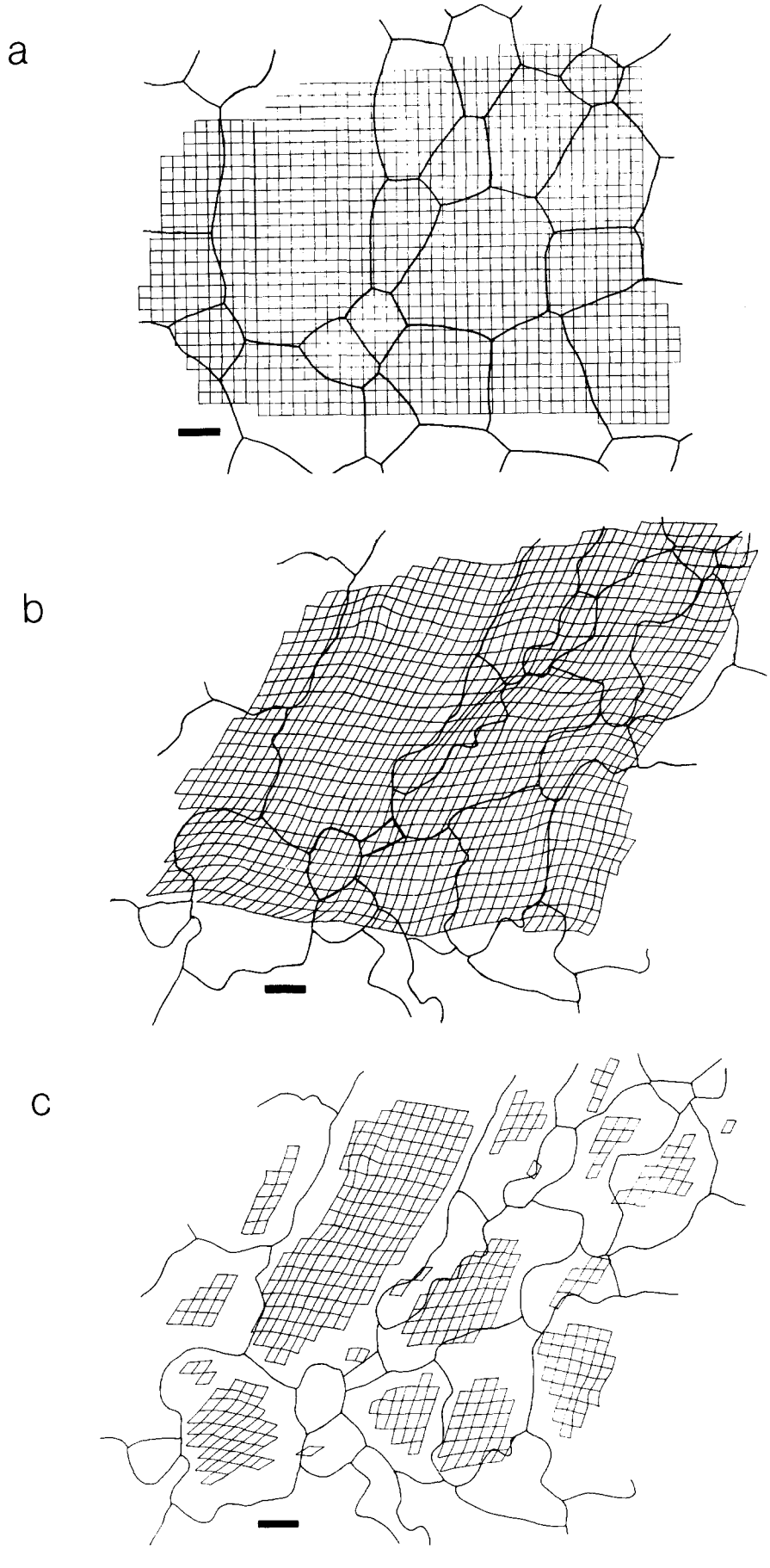

Fig. 10. Strain maps for experiment TO-65. (a) Arbitrarily positioned orthogonal grid superimposed on a map of the grain boundaries in the undeformed state. (b) Deformed grid as calculated using marker particles superimposed on the map of the positions of grain boundaries in the deformed state. (c) Deformation grid showing only those grid intersections which could be calculated without using triads of marker particles that cross grain boundaries. Compare with Figs. 8(a) and (c). Scale bars represent 0.1 mm.

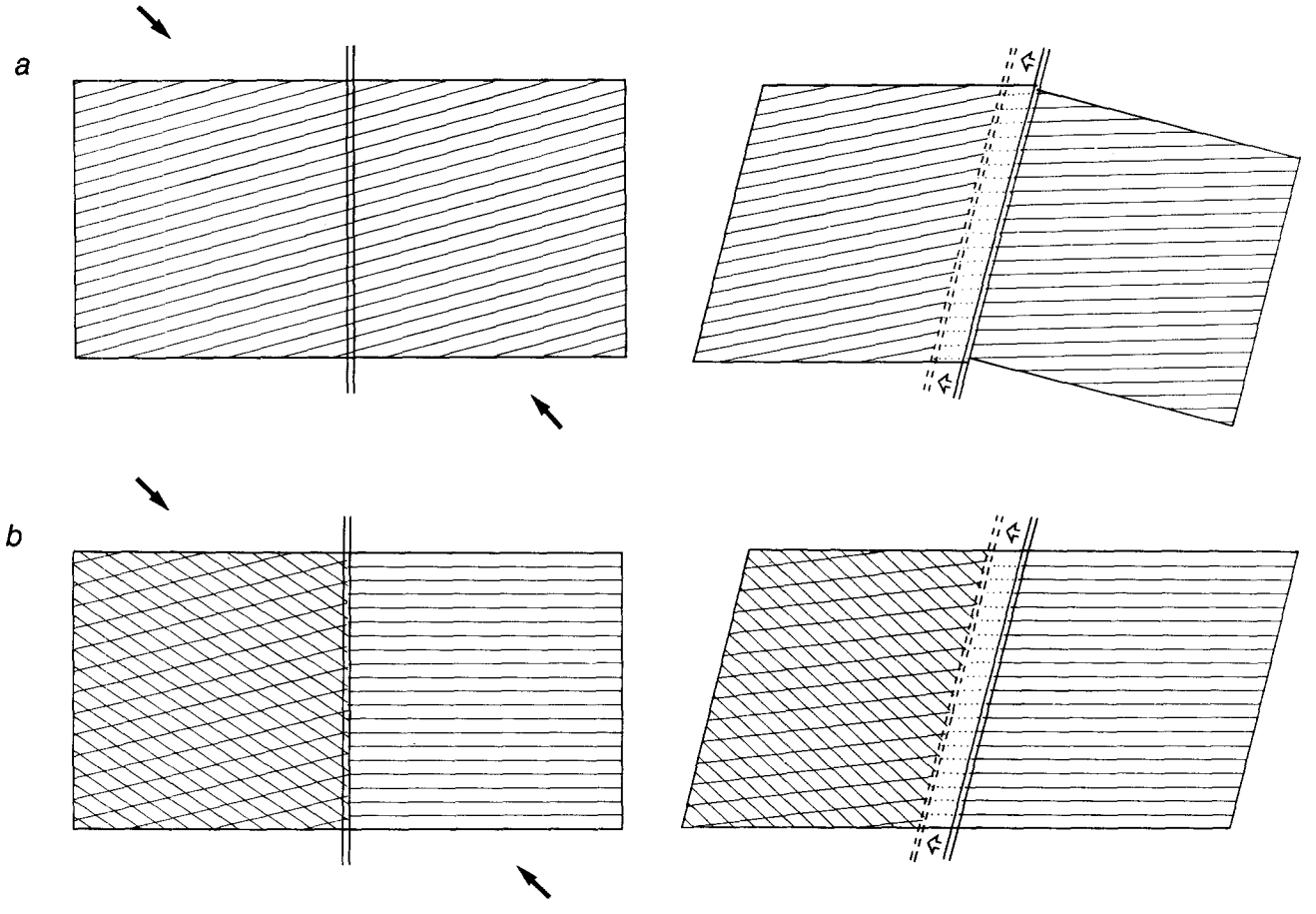

Fig. 11. (a) Model depicting the predicted sense of motion of a grain boundary that separates two grains of roughly equal orientation that undergo different strains. (b) Model depicting the predicted sense of motion of a grain boundary separating two grains with different initial orientations that undergo the same strain. Multiple parallel lines symbolize lattice planes, which become dashed when reoriented by a migrating grain boundary. Heavy double lines symbolize a grain boundary, whose migrated position is dashed. It should be noted that the grain boundary in (a) is allowed to be materially non-coherent.

distributed, and although grain boundary energy can be seen at work locally keeping grain boundary triple junctions at 120 degrees (Urai *et al.* in press), there is no tendency for larger grains to grow at the expense of their neighbours, as would be expected if grain boundary energy was the dominant driving force. Large elastic strains do not appear to be locked into the grains, although it is possible that they may be important at the very earliest stages of the deformation. This leaves lattice defect energy as the other potential driving force.

Since the dislocation density could not be measured in these experiments it is worthwhile considering two simple cases that together provide the basis for a lattice defect energy driven model in materials with a limited number of available slip systems. The first case, as depicted in Fig. 11(a) consists of two adjacent grains with similar crystallographic orientations with respect to the stress field. Prior to the deformation they had equal dislocation densities. These grains are separated by a grain boundary, across which there is a marked contrast in total slip activity. The reasons for this activity contrast are unimportant to this model. In this case the increase in lattice defect energy in the more active grain results in the grain boundary migrating towards this grain. The idea of strain-induced boundary migration is common to both the metallurgical and geological literature (Bailey & Hirsch 1962, Poirier & Guillope 1979), and the model can be readily translated into terms of strain to imply that if two grains have the same orientation, the more intensely strained grain will be consumed by its neighbour, and thus a function related to the intra-grain strains can be used to predict grain boundary migrations. In the second case, as depicted in Fig. 11(b), the two grains again start off with equal dislocation densities, but they are equally strained, the difference in lattice defect energy coming from the difference in crystallographic orientations in the two grains. One grain is well oriented for single slip on a soft glide system, while the other grain has several slip systems activated by the stress field, resulting in more dislocation tangles and thus a higher dislocation density. This type of behaviour has been postulated for camphor by Urai & Humphreys (1981). In this case the 'better' oriented grain grows at the expense of its neighbour.

It now becomes necessary to define precisely what a "well-oriented" grain is. Since it is known from experiments such as TO-63 that in OCP the dominant preferred orientation that develops is one with the basal plane in an orientation parallel to a plane of maximum resolved shear stress, it seems reasonable to assume that this may

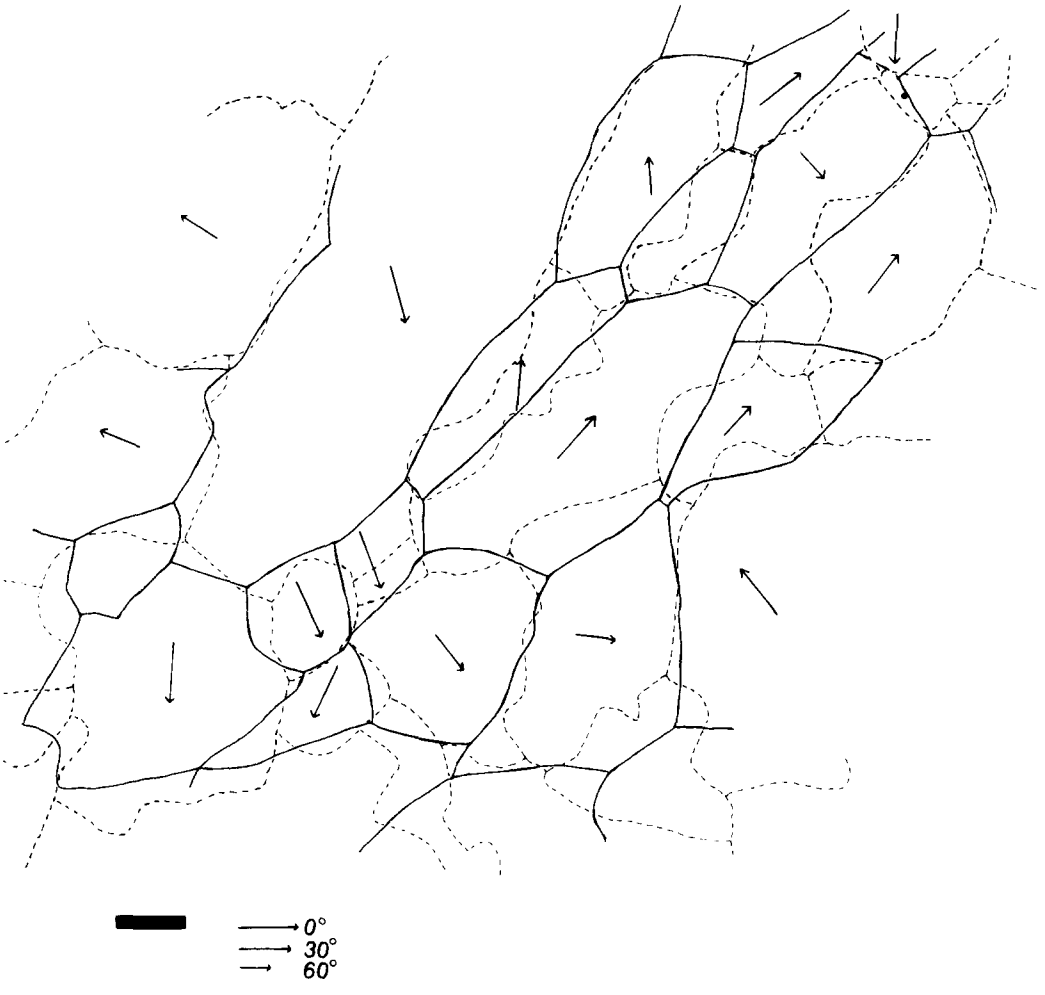

Fig. 12. Boundary migration map for experiment TO-65. Positions in the deformed state of material lines coincident with grain boundaries in the undeformed state (solid lines), together with the real grain boundary positions in the deformed state (dashed lines). Arrows show dip direction and are proportional in length to the dip of the basal plane for each grain in the undeformed state. Scale bar represents 0.1 mm.

represent the orientation of a "well-oriented" grain. One approach to developing an orientation function is thus to assume that it will be related to the resolved shear stress on the basal plane. On this basis it becomes possible to produce an orientation function such as $\sin 2\xi \cdot \sin \phi$, where ξ is the angle between the slip plane normal and the major stress axis and ϕ is the angle between the slip plane normal and the intermediate stress axis. The major and minor stress axes are assumed to be at 45° to the frosted grips and the intermediate stress axis is assumed to be normal to the plane of the glass glides.

Once functions exist for the two cases already stated it becomes necessary to generalize the model to include the more useful situations where one grain is more intensely strained, and either worse or better oriented with respect to its neighbour. The former case is clear, the boundary should migrate towards the more highly strained, worse-oriented grain. Unfortunately it is not at all clear how the two principal cases should be combined in the latter case. This model, though simple, has the virtue of being testable within the framework of the experimental procedure already available, and results of this testing are presented in the following section.

Model test

In order to test a model of grain boundary migration it is necessary to observe absolute motions of grain boundaries, that is the part of the motion relative to material lines, ignoring that portion imparted by the strain field. The method chosen to observe absolute motions was to calculate the positions, in the deformed state, of the material lines that coincided with grain boundaries in the undeformed state. These positions could be calculated in the same manner as the imaginary orthogonal grid, and are shown, together with the real positions of grain boundaries in the deformed state, in Fig. 12.

Of some 80 grain boundaries available for study from experiments TO-64 and TO-65, 49 fulfilled the criterion for analysis, namely that the strain state on both sides of the boundary could be calculated and the crystallographic orientations of both grains were recorded (Table 2). Of these, 37 displayed an appreciable grain boundary migration, and these boundaries provide the basis for testing the model proposed earlier.

The basic assumptions about lattice defect energy that led to the model are that higher strains produce more defects, that 'worse' orientations produce more defects,

Table 2. Compilation of data used to test model

	Grain A				Grain B					
S_1	Plunge (degrees)	Plunge direction (degrees)	OF	Energy function	S_1	Plunge (degrees)	Plunge direction (degrees)	OF	Energy function	Differential energy	Actual GBM
Experiment TO-64											
1.55	48	077	0.601	0.60	1.25	32	345	0.734	0.42	−0.19	−6.5
1.45	55	110	0.439	0.70	1.72	54	081	0.559	0.71	0.01	6.5
1.23	50	108	0.520	0.53	1.25	37	333	0.469	0.58	0.05	5.2
1.23	50	108	0.520	0.53	1.38	37	057	0.325	0.79	0.25	4.5
1.25	37	333	0.469	0.58	1.29	3	003	0.993	0.32	−0.25	−8.1
1.25	37	333	0.469	0.58	1.24	27	014	0.787	0.39	−0.19	−6.1
1.72	54	081	0.559	0.71	1.31	30	027	0.509	0.58	−0.13	−8.4
1.31	18	009	0.905	0.36	1.31	30	027	0.509	0.58	0.21	−2.6
1.31	18	009	0.905	0.36	1.25	22	206	0.571	0.51	0.15	0.0
1.09	47	058	0.299	0.65	1.25	40	006	0.749	0.41	−0.24	−1.9
1.38	37	057	0.325	0.79	1.25	40	006	0.749	0.41	−0.38	−11.3
1.29	3	003	0.993	0.32	1.31	30	027	0.509	0.58	0.25	5.5
1.29	3	003	0.993	0.32	1.35	27	194	0.787	0.42	0.10	1.0
1.31	30	027	0.509	0.58	1.35	27	194	0.787	0.42	−0.15	−5.5
1.25	40	003	0.762	0.40	1.35	27	194	0.787	0.42	0.02	−1.9
1.25	40	006	0.749	0.41	1.14	44	059	0.338	0.64	0.23	0.3
1.31	18	009	0.905	0.36	1.35	53	098	0.579	0.54	0.18	0.0
1.35	53	098	0.579	0.54	1.25	22	206	0.571	0.51	−0.04	0.0
Experiment TO-65											
1.37	43	302	0.321	0.79	1.36	13	164	0.826	0.41	−0.38	−1.6
1.37	43	302	0.321	0.79	1.40	46	292	0.500	0.62	−0.16	0.0
1.18	13	164	0.826	0.35	1.43	38	356	0.780	0.45	0.10	1.6
1.36	13	164	0.826	0.41	1.40	46	292	0.500	0.62	0.21	−2.3
1.36	13	164	0.826	0.41	1.50	35	006	0.801	0.46	0.05	2.6
1.36	13	164	0.826	0.41	1.21	16	184	0.952	0.32	−0.09	−1.9
1.36	13	164	0.826	0.41	1.41	0	159	0.743	0.46	0.06	6.8
1.43	38	356	0.780	0.45	1.23	31	053	0.236	0.80	0.35	−1.9
1.43	38	356	0.780	0.45	1.50	35	006	0.801	0.46	0.01	3.2
1.23	31	053	0.236	0.80	1.29	34	184	0.821	0.39	−0.42	−1.0
1.23	31	053	0.236	0.80	1.24	57	138	0.057	1.11	0.31	3.2
1.29	34	184	0.821	0.39	1.24	57	138	0.057	1.11	0.72	0.0
1.50	35	006	0.801	0.46	1.41	0	159	0.743	0.46	0.00	0.0
1.50	35	006	0.801	0.46	1.37	17	042	0.100	1.13	0.67	2.6
1.24	57	138	0.057	1.11	1.35	35	038	0.198	0.94	−0.17	0.0
1.24	57	138	0.057	1.11	1.37	17	042	0.100	1.13	0.02	0.0
1.35	35	038	0.198	0.94	1.50	47	042	0.071	1.31	0.37	3.2
1.52	16	184	0.952	0.40	1.85	15	196	0.819	0.56	0.16	4.8
1.41	0	159	0.743	0.46	1.37	17	042	0.100	1.13	0.67	−1.0
1.41	0	159	0.743	0.46	1.28	42	141	0.155	0.96	0.50	0.0
1.37	17	042	0.100	1.13	1.50	47	042	0.071	1.31	0.17	−1.9
1.37	17	042	0.100	1.13	1.28	42	141	0.155	0.96	−0.17	4.8
1.37	17	042	0.100	1.13	1.31	49	097	0.637	0.49	−0.64	−6.5
1.50	47	042	0.071	1.31	1.12	13	320	0.169	0.82	−0.49	−2.6
1.85	15	196	0.819	0.56	1.28	42	141	0.155	0.96	0.40	1.6
1.28	42	141	0.155	0.96	1.31	49	097	0.637	0.49	−0.47	0.0
1.31	49	097	0.637	0.49	1.12	13	320	0.169	0.82	0.33	0.0
1.08	0	154	0.616	0.41	1.41	0	159	0.743	0.46	0.05	0.6
1.08	0	154	0.616	0.41	1.85	15	196	0.819	0.56	0.15	0.0
1.36	13	164	0.826	0.41	1.08	0	154	0.616	0.41	0.01	1.6
1.52	16	184	0.952	0.40	1.08	0	154	0.616	0.41	0.01	1.9

and that unstrained grains have few defects, regardless of orientation. The simplest function that combines the strain and orientation functions and fits these assumptions is S_1/OF, where S_1 is the principal stretch, and OF is the orientation function $\sin 2\xi \cdot \sin \phi$. Since the relative importance of these two parameters is completely unknown, various weighting functions were added to give greater importance to one or the other. The function that worked the best, although not significantly better than several other versions, is the one used here, namely $S_1/(OF + 1)^2$. The model as formulated then simply predicts that the boundary will move towards the grain with the lower energy function. The strains, average grain orientations for the period of the experiment and the resulting energy functions are displayed in Table 2, together with the resulting migration predictions and real migrations, for both experiments.

To test the basic validity of the model those 18 boundaries for which one grain had both the higher orientation function and the lower measured strain are first considered. Of these the model correctly predicts the migration direction of 16 boundaries. Out of the total set of 37 boundaries the model correctly accounts for the migration direction of 30 boundaries. Perhaps of most significance is the fact that of the 21 boundaries with the largest absolute grain boundary motions, the model correctly accounts for 19 of these motions.

A more rigorous test of this model is shown in Fig. 13,

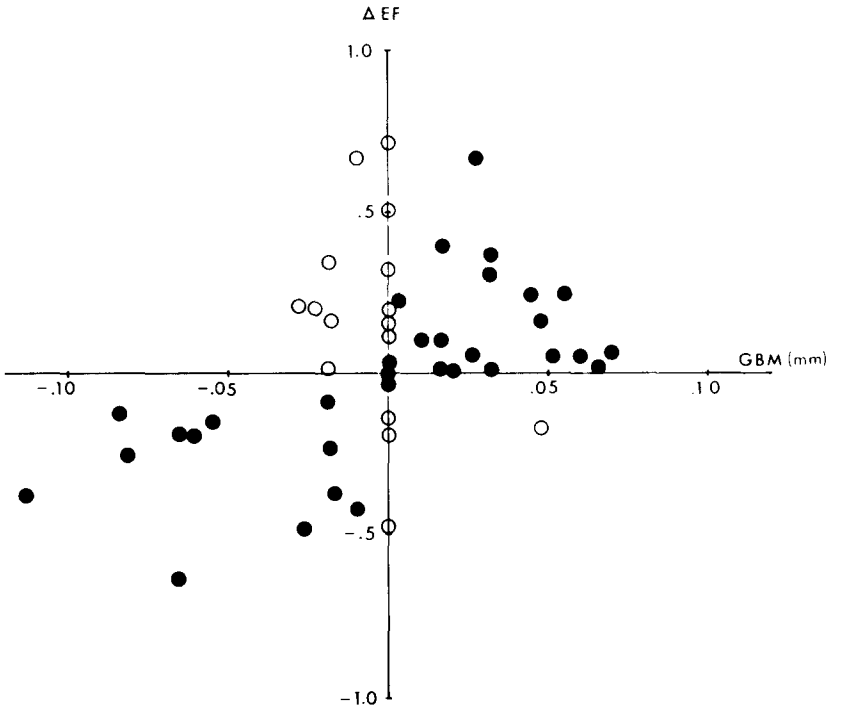

Fig. 13. Graph plotting the difference between the predicted energy levels and the actual average grain boundary motions, for experiments TO-64 and TO-65. Those points that fall in quadrants I and III (filled circles), indicate grain boundaries whose sense of motion is correctly accounted for by the model. The sign of the grain boundary migration (GBM) and energy function (ΔEF) merely depends on which grain is chosen for reference.

which is a graph of absolute grain boundary migration, in this case including 12 static boundaries, vs the difference between the energy functions for each grain. It can be seen that the precise relationship between the energy function contrast and grain boundary migration has not yet been determined, but also that this model accounts for the essential behaviour of mobile grain boundaries in these experiments. As an indication of the relative importance of strain contrasts vs orientation contrasts it is worth noting that 70% of the grain boundary motions can be accounted for by considering only the influence of orientation. However, the importance of contrasts in internal strains could well increase in more intensely deformed samples.

CONCLUSIONS

Although these results apply strictly only to the deformation of OCP under the stated experimental conditions, if they are assumed to be of more general validity, they have many implications for fabric development in dynamically recrystallizing aggregates of minerals of low crystallographic symmetry. It is clear that grain boundary migrations and lattice reorientations act semi-independently to modify existing fabrics.

The model presented, apart from correlating well with specific grain boundary kinematics, can also be used to account for a number of experimental observations. It provides a mechanism for the development of the *c*-axis point maxima found in the experiments. Lister & Snoke (1984) suggest that recrystallization can have the effect of "resetting the finite strain clock", that is forcing the grain shape foliation to lag behind the orientation of maximum finite elongation. The maximum amount of resetting of this type that could take place would result in a foliation parallel to the orientation of maximum incremental strain, and even this could only be achieved with a very high grain boundary migration rate with respect to the strain-rate. In experiment TO-63 the foliation that develops is 5° behind the orientation of maximum incremental strain, and thus the process suggested by Lister & Snoke (1984) would in this case have to be supplemented by another, unknown, process. Selective consumption of subgrains, as mentioned earlier, can also be accounted for in this model. The model further predicts that with progressive crystal plastic reorientations in two grains, it is possible that the relative magnitudes of their energy functions would reverse, and thus so would the direction of grain boundary migration. Oscillating boundaries have been observed in OCP, although it is not known if they are a result of this process.

The success of the model is related to the demonstration of the importance of lattice orientation and intragrain strains in controlling grain boundary migration. However, the implication that the driving force is the dislocation density contrast is not in itself strengthened by these experiments as no observations of dislocations were made. As OCP etches readily in air, a more direct test of this hypothesis may be possible. On a statistical level a predictive model for fabric development could be based on whatever crystal plastic lattice rotation model is favoured, plus the effects of grain boundary migration.

Such a combination model promises to explain the major features of fabric diagrams, the girdles and the point maxima. In summary:

(1) Grain boundary migration can have a constructive modifying effect on the development of a crystallographic preferred orientation in materials of low symmetry.

(2) Grain boundary migration appears to be controlled by a combination of the relative orientations and internal strain states of adjacent grains, possibly via the lattice defect energy contrasts that these factors induce.

(3) It should be possible to develop a predictive model of fabric development in polycrystals of low symmetry in regimes favourable to crystal plastic glide and dynamic recrystallization.

Acknowledgements—I would like to thank W. D. Means, J. L. Urai and B. Bayly for numerous helpful ideas and suggestions, and L. Bouzida for her help in proofreading. C. J. L. Wilson helped clarify many points at the review stage. This work was undertaken with the aid of a Presidential Fellowship from the State University of New York at Albany, together with funding from National Science Foundation grants EAR 8306166 and EAR 820582001.

REFERENCES

Bailey, J. E. & Hirsch, P. B. 1962. Recrystallisation processes in some polycrystalline metals. *Proc. R. Soc.* **A267**, 11–30.

Etchecopar, A. 1977. A plane kinematic model of progressive deformation in a polycrystalline aggregate. *Tectonophysics* **39**, 121–139.

Friedman, M. & Higgs, N. G. 1981. Calcite fabrics in experimental shear zones. In: *Mechanical Behavior of Crustal Rocks. Am. geophys. Un. geophys. Monogr.* **24**, 11–27.

Hudleston, P. J. 1980. The progressive development of inhomogeneous shear and crystallographic fabric in glacial ice. *J. Struct. Geol.* **2**, 189–196.

Jensen, L. N. 1984. Quartz microfabric of the Laxfordian Canisp Shear Zone, NW Scotland. *J. Struct. Geol.* **6**, 293–302.

Lister, G. S., Paterson, M. S. & Hobbs, B. E. 1978. The simulation of fabric development during plastic deformation and its application to quartzite: the model. *Tectonophysics* **45**, 107–158.

Lister, G. S. & Price, G. P. 1978. Fabric development in a quartz–feldspar mylonite. *Tectonophysics* **49**, 37–78.

Lister, G. S. & Snoke, A. W. 1984. S–C Mylonites. *J. Struct. Geol.* **6**, 617–638.

Means, W. D. 1983. Micromotion and microstructure in recrystallisation flow of octachloropropane, a first look. *Geol. Rdsch.* **72**, 511–528.

Means, W. D. & Xia, Z. G. 1981. Deformation of crystalline materials in thin sections. *Geology* **9**, 538–543.

Mercier, J.-C., Anderson, D. A. & Carter, N. L. 1977. Stress in the lithosphere: inferences from steady-state flow of rocks. *Pure appl. Geophys.* **115**, 199–226.

Poirier, J.-P. & Guillope, M. 1979. Deformation induced recrystallisation of minerals. *Bull. Mineral.* **102**, 67–74.

Ramsay, J. G. 1967. *Folding and Fracturing of Rocks.* McGraw-Hill, New York.

Tungatt, P. D. & Humphreys, F. J. 1981. An in-situ optical investigation of the deformational behaviour of sodium nitrate—an analogue for calcite. *Tectonophysics* **78**, 661–675.

Twiss, R. J. 1977. Theory and application of a recrystallized grain size palaeopiezometer. *Pure appl. Geophys.* **115**, 224–227.

Urai, J. L. 1983. Deformation of wet salt rocks. Unpublished Ph.D. thesis, University of Utrecht.

Urai, J. L. & Humphreys, F. J. 1981. The development of shear zones in polycrystalline camphor. *Tectonophysics* **78**, 677–685.

Urai, J. L., Means, W. D. & Lister, G. S. in press. Dynamic recrystallisation of minerals. *Am. geophys. Union. geophys. Monogr.*

Wakahama, G. 1964. On the plastic deformation of ice—6. Plastic deformation of polycrystalline ice. *Low Temp. Sci. A***22**, 1–24.

Wilson, C. J. L. 1984. Shear bands, crenulations and differentiated layering in ice–mica models. *J. Struct. Geol.* **6**, 303–319.